Calibration techniques for imaging FTIR data

Christoph C. Borel, William B. Clodius and Steven P. Love
Space and Remote Sensing Sciences Group Los Alamos National Laboratory
Los Alamos, NM 87545, USA

ABSTRACT

Full utilization of hyper-spectral imagery in the thermal infrared region requires a high-quality calibration, and the calibration quality requirement increases with the power and sophistication of the retrieval algorithms to be employed. Here we examine calibration issues associated with an airborne imaging Michelson Fourier Transform Infrared (FTIR) Spectrometer operating in the long-wave infrared (LWIR) region. In addition to the fundamental challenge of extracting a weak signal of interest from a complex background, problems which arise in such an instrument include pointing jitter, detector non-linearity, sampling position errors and etalon effects within the focal plane array. In each case, a frequent, high-quality calibration can ameliorate these problems. We discuss several hyper-spectral data analysis techniques, and how our calibration strategy, incorporating both ground and on-board calibration systems, improves the sensitivity of the retrievals.

Keywords: Fourier Transform Infrared Radiometer, Hyperspectral Infrared Imaging, Calibration, Artifact Removal

1. INTRODUCTION

The thermal infrared region from 8 to 14 μm is often called the "fingerprint" region to detect, identify and quantify gases in the atmosphere. Simple molecules such as water vapor (H_2O), sulfur dioxide (SO_2), methane (CH_4), ammonia (H_3N), sulfur hexafluoride (F_6S), etc. have narrow spectral absorption lines of widths less than 0.1 cm^{-1} which can be resolved using conventional dispersive imaging spectrometers which have reported fixed resolutions of 2-5 cm^{-1} in the 7.5 to 13.5 μm range, e.g. Hackwell et al, 1996. In contrast FTIR's have variable spectral resolution proportional to the inverse of the optical path difference which allows high-spectral resolutions better than 0.1 cm^{-1}, Beer, (1991). Other advantages of imaging FTIR's are: (1) More light throughput due to the missing slit and fewer optical surfaces, (Throughput or Jacquinot's advantage); (2) Light is not separated into bands and each wavelength of light is sampled many times (Multiplex or Fellgett's advantage); (3) Spectral calibration is "built" in by using helium-neon lasers to measure the mirror position (Frequency precision or Conne's advantage); (4) Spectral resolution is constant across the spectral region of interest and well suited to measuring atmospheric lines; (5) Time-variable events like gas plumes can be imaged using the image frame sequences to determine wind-speeds.

There are also disadvantages to using FTIR's: (1) The large signal causes a large photon background noise; (2) Compensated FTIR's need a large dynamic range due to the near doubling of the intensity in the center-burst; (3) Un-compensated or dispersive FTIR's have frequency dependent path differences which broaden the center-burst and require full two-sided interferograms; (4) Pointing jitter affects spatial resolution and if high in frequency the spectra; (5) Internal reflections in the detector cause interferences or channeling which can be hard to remove through calibration; (6) Non-linear detector responses cause systematic temperature offsets and require more calibration sources; (7) Random or periodic sampling position errors coupled with non-linearity cause systematic and random temperature errors; (8) Dead or noisy pixels must be corrected before pointing jitter can be removed; (9) Imaging FTIR's need to stare at a scene for one mirror-scan to acquire a spectrum limiting the sensors field of view to the number of detectors.

Here are some solutions to those real-world problems: (1) Dispersion reduces the dynamic range of center-burst thus requiring fewer quantization levels (Griffiths and de Haseth, (1986)). (2) Phase corrections using complex FFT's reduce the broadening of the center-burst, improve the Signal to Noise Ratio (SNR) and when done inside the instrument reduce the required number of samples by a factor of two. (3) De-jittering of frames of interferogram improves sharpness. (4) Channel masking before performing the Fast Fourier transform (FFT) reduces ringing in the spectral domain. (5) Non-linearity correction minimizes spectral harmonics.

2. A FLEXIBLE FTIR MODEL

We have developed a flexible and simple FTIR model, shown in Fig. 1), to investigate some of the above mentioned "real-world" problems of FTIR's. Fig. 1. The parameters used for our simulations are:

Further author information: (Send correspondence to C.C.B.)
C.C.B.: E-mail: cborel@lanl.gov; WEB: nis-www.lanl.gov/~borel; Telephone: (505) 667-8972; Fax: (505) 667-3815
W.B.C.: E-mail: wclodius@lanl.gov S.P.L.: E-mail: splove@lanl.gov

Imaging Spectrometry VII, Michael R. Descour, Sylvia S. Shen, Editors,
Proceedings of SPIE Vol. 4480 (2002) © 2002 SPIE · 0277-786X/02/$15.00

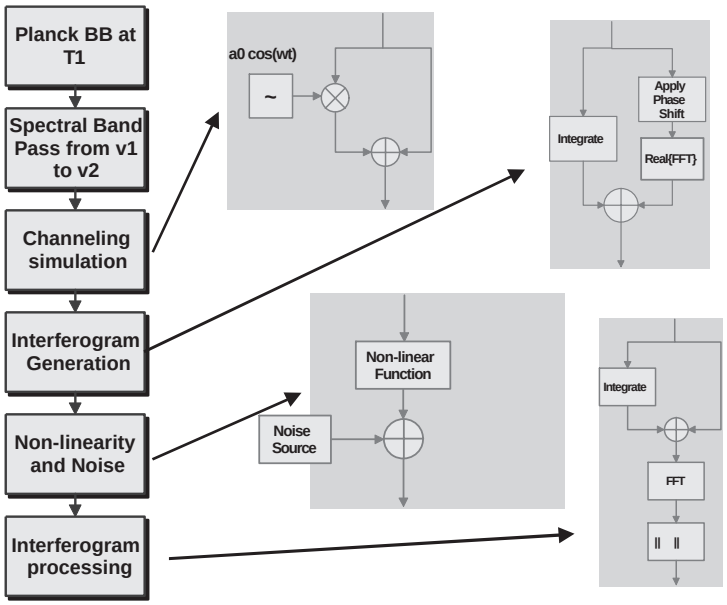

Figure 1. Block-diagram of a simple FTIR model.

- Signal to Noise Ratio $SNR = 1000$, number of samples $N_f = 4096$ frames, a responsivity between 750 and 1250 cm^{-1} (in-band), and spectral sampling of 2 cm^{-1}.
- Phase dispersion model: $\phi(\nu) = 500(\frac{\nu}{\nu_{max}})[1 + 0.3(\frac{\nu}{\nu_{max}})^2]$.
- Channeling amplitude: $A(\nu) = (1. + 0.2\cos(\omega_0 \nu))$.
- Nonlinear model: $DN(\text{nonlinear}) = \text{DN(linear)}^{\text{d}}$ where $d = 0.33$.
- Relative position sampling errors in sample units:
  - Periodic: $\Delta Z_p(z) = a_0 \sin(2\pi \frac{z}{\delta z})$,
  - Random: $\Delta Z_r(z) = b_0 N(m = 0, \sigma = 1) \otimes LP - filter(\nu_{cutoff} = 0.1\nu_{max})$,

  where a_0 and b_0 are selected so that the standard deviation $STDEV(\Delta Z_p) = 0.02$ and $STDEV(\Delta Z_r) = 0.001$ of a sampling distance.
- 3 calibration sources at temperatures $T_0 = 20^o\ C, T_1 = 30^o\ C$ and $T_2 = 40^o\ C$,

Using this simple FTIR model we simulate the effect of phase errors, channeling and non-linearity on the 2-point calibration error for the middle black body (BB_1).

2.1. 2-point calibration

Let $I_k(x, i, j)$ be the interferogram of the k-th calibration source at T_k.

We define the measured spectral response (MSR) at the (i, j) pixel as: $MSR_k(\nu, i, j) = |FFT[I(x, i, j)]|$. Given Planck's function $B()$, the calculated BB radiance for T_k is $CBB_k(\nu) = B(\nu, T_k)$. Assuming a linear detector, the 2-point calibrated radiance $L_1(\nu)$ of BB_1 is:

$$L_1(\nu) = \frac{MSR_1 - a(\nu, i, j)}{b(\nu, i, j)}$$

where $a(\nu, i, j) = MSR_0(\nu, i, j) - b(\nu, i, j)CBB_0(\nu)$, and $b(\nu, i, j) = \frac{MSR_2(\nu,i,j) - MSR_0(\nu,i,j)}{CBB_2(\nu) - CBB_0(\nu)}$.

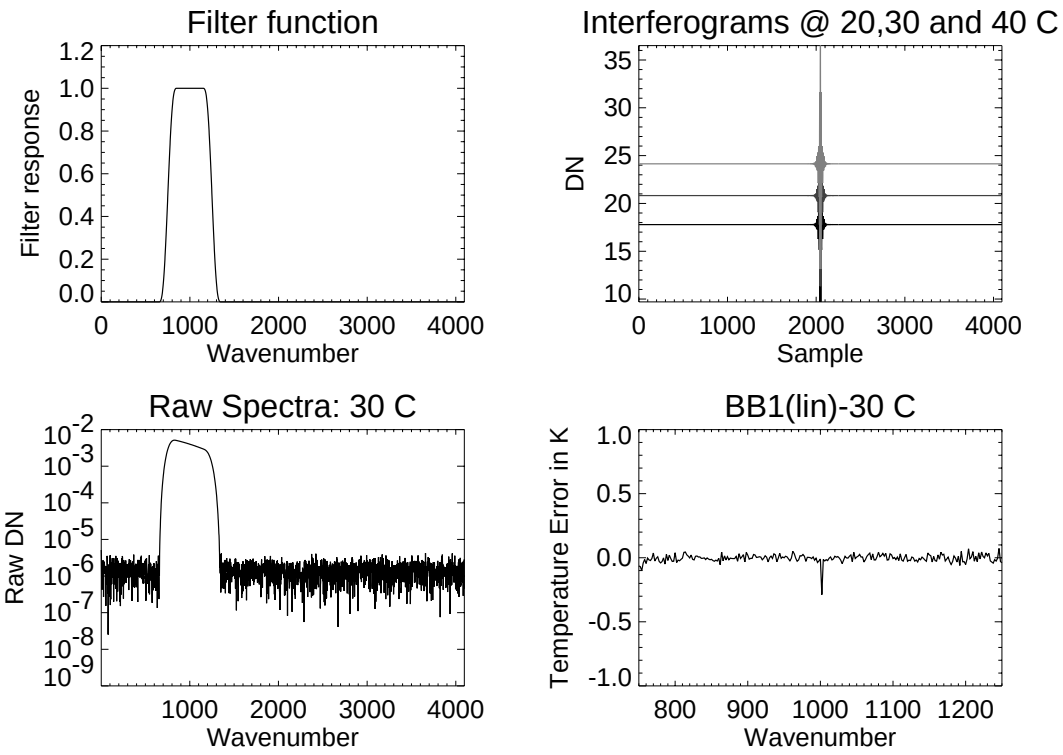

Figure 2. Filter function (UL), interferograms for 20^o, 30^o and 40^o C black-bodies (UR), the raw digital number (DN) spectrum for the 30^o C black-body with noise (LL), and the temperature error for the 2-point calibrated 30^o C black-body (LR).

2.2. Linear FTIR simulation

In Fig. 2 we show the simulated linear FTIR. Note the strongly peaked symmetric center-burst and the symmetry which allow the acquisition of one-sided interferograms.

2.3. Linear + dispersion FTIR simulation

We now add a non-linear phase to the model and obtain a a asymmetric center-burst as shown in Fig. 3 which requires a two-sided interferogram to capture the spectrum. Note that the dynamic range is reduced compared to the undispersed FTIR. This feature has been used to reduce the linearity requirements on detectors and the number of quantization bits (Griffiths and de Haseth, 1986). Phase errors can also be introduced when (1) the beamsplitter and compensator plate are not identical or mis-aligned and (2) in rapid scan systems where the finite bandwidth of the sensor causes phase shifts (Beer, 1992).

2.4. Linear + dispersion + channeling FTIR simulation

Channeling is caused by multiple reflections in the optical path between closely spaced surfaces or thin plates, see Fig. 1. Channeling causes ghosts of the center-burst symmetrically offset from the center. Assuming the channeling is caused by a thin plate with wavelength independent refractive index, we can model channeling in the spectral domain as amplitude modulations as shown in Fig. 4 (UL).

2.5. Non-linear + dispersion + channeling FTIR simulation

The non-linearity produces spectral harmonics which occur at the sum and differences of the in-band wavenumbers. There is a corresponding apparent non-zero mean temperature offset on BB_1 and increased temperature noise compared to linear FTIR's as shown in Fig. 5.

2.6. Non-linear + dispersion + channeling + sampling position error FTIR simulation

Sampling position errors result in phase-modulations of the signal. With a periodic sampling position error $\Delta Z_p(z)$ and $SNR = \infty$, the temperature error consists of offset (for the non-linear case only) and low-frequency components as shown in Fig. 6. Periodic sample position errors generate ghosts of spectral lines, e.g. Learner et al, 1996. A potential mechanism to obtain a periodic sample position error is cross-talk from inadequately

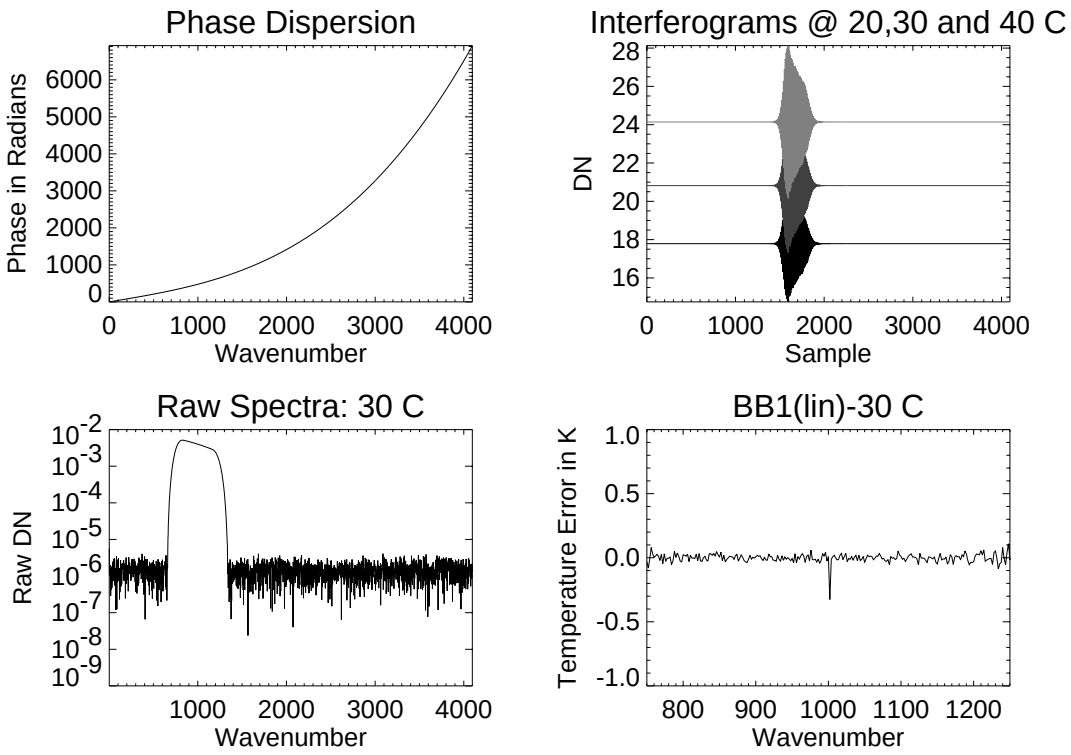

Figure 3. Phase function $\phi(\nu)$ (UL), interferograms for 20^o, 30^o and 40^o C black bodies (UR), the raw digital number (DN) spectrum for the 30^o C black-body with noise (LL), and the temperature error for the 2-point calibrated 30^o C black-body (LR).

smoothed power supplies which can add a spurious periodic signal to the laser reference signal which is used to trigger sampling of the detector.

With a random sampling position error $\Delta Z_r(z)$ and $SNR = \infty$, the temperature error consists of offset (for the non-linear case only) and low-frequency components as shown in Fig. 7.

The band averaged (from 750 to 1250 cm^{-1}) RMS error of the temperature is a strong function of the RMS of the sample position as shown in Fig. 8. For sample position RMS errors of greater than 1/1000 of a sample the temperature error is dominated by sample position errors. When the RMS of the sample position error exceeds 1/10 th of a sample the temperature fluctuations are 1 deg K for a linear and 10 K for the nonlinear case. In Fig. 9 we plot the spectral temperature error as a function of wavenumber and standard deviation of the sample position error. Thus it is extremely important to mitigate mechanically introduced sample position errors in imaging FTIR's which can be accomplished by (1) triggering the detectors using the HeNe fringes or (2) measuring the position of the mirror at the time of integration.

Another source of sample position errors which is much harder to control are air temperature variations between the two arms of the interferometer (Manning and Griffith, 1997). Potential sources for temperature fluctuations include the interferometer are: (1) waste heat from reference laser, (2) calibration sources, (3) power supply, (4) electronic components, (5) piezo actuators used for dynamic alignment and (6) linear translation mechanism to move the mirror. Usually an imaging FTIR is calibrated less often than data is taken. The operating temperatures for the instrument can change the spectrometer response $a(\nu, i, j)$ and $b(\nu, i, j)$. In a commercial instrument (Digilab FTS-60A) response variations of up to 4% per deg K were observed (MacBride et al, 1997). Several mechanisms are responsible for these drifts, (1) temperature variations in spectrometer source, (2) change of beamsplitter throughput with temperature, (3) mirror temperatures and (4) drift in detector temperatures.

3. RADIOMETRIC CORRECTIONS

As mentioned, some of the FTIR artifact's can be corrected and the radiometry improved. Phase error correction will not be discussed here. For a summary of phase error correction methods see Bell, 1972.

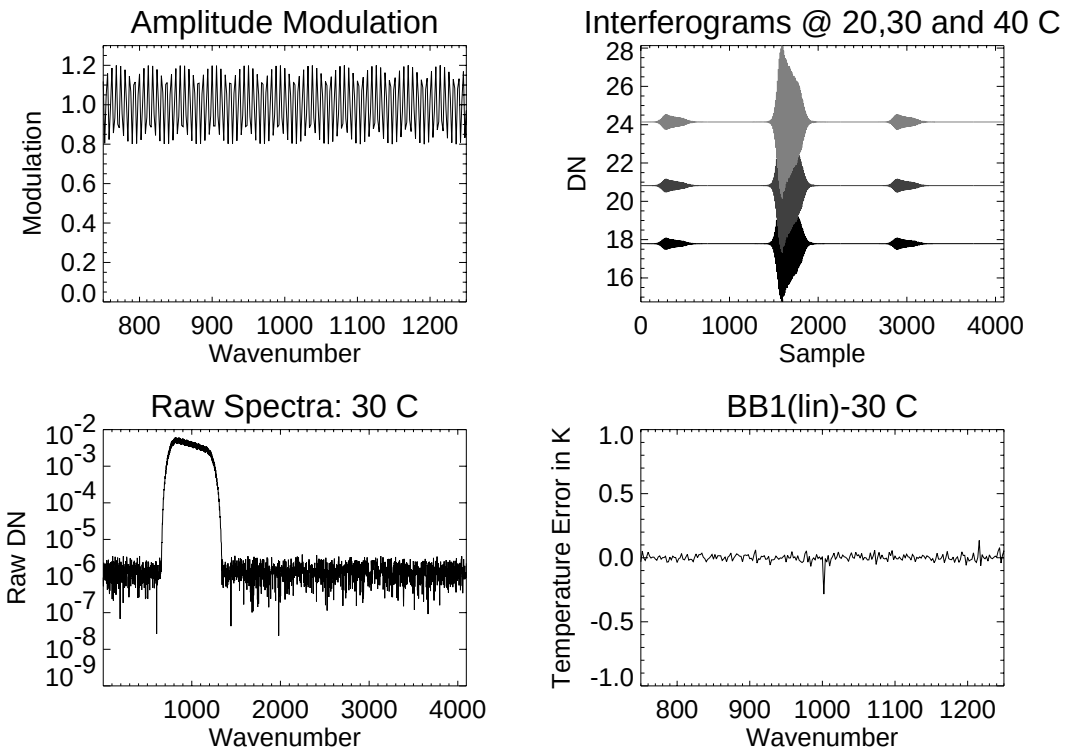

Figure 4. Modulation function $A(\nu)$ (UL), interferograms for 20^o, 30^o and 40^o C black-bodies (UR), the raw digital number (DN) spectrum for the 30^o C black-body with noise (LL), and the temperature error for the 2-point calibrated 30^o C black-body (LR).

3.1. Channeling effect correction

A simple method to correct channeling is to cut off (apodize) the channeling bursts which removes the strong oscillation in the spectral domain. Apodizing the channeling bursts eliminates the sinusoidal modulation in the spectral domain. Removing the channeling, however, increases the Amplitudes of the instrument functions side lobes. This causes ringing near narrow spectral features, e.g. atmospheric absorption lines and has to be taken into account in the data exploitation. We found that if the FTIR is linear and stable between calibrations and data acquisitions the channeling can be removed with a 2-point calibration.

3.2. Sample position corrections

To correct sample position errors an accurate measurement of the mirror position for each frame must be available. Only recently have such measurements been used to correct sample position errors, e.g. Palchetti and Lastrucci, 2001. The following steps were used to correct sample position errors for the simple FTIR: (1) Generate a interferogram with a simulated random position error $\Delta Z_r(z)$. (2) Simulate a non-ideal laser reference system which measures the mirror position $\Delta \hat{Z}_r(z) = \Delta Z_r(z) + N(0, \sigma_z)$, where σ_z is the sample position measurement error. (3) Re-sample the simulated interferogram to equal distant samples using cubic spline interpolation. (4) Calibrate the black-body $BB2$. This method reduces the additional noise introduced by the sample position error as long as the measurement error is less than about 1/10 of the sample position error, e.g. if $STDEV(\Delta Z_r) = 0.01$ then $\sigma_z = 0.001$.

3.3. Non-linear response correction

In Fig. 10 we show a block-diagram of how the non-linearity of a detector can be corrected using an adaptive compensator. A simple method to retrieve the exponent d for the non-linear model $y = x^d$ is to maximize the ratio:

$$R = \frac{max\{\text{In} - \text{band} \;\; \text{Signal}\}}{\sigma\{\text{Out} - \text{of} - \text{band} \;\; \text{Signal}\}},$$

where the In-band is from 750 to 1250 cm^{-1}.

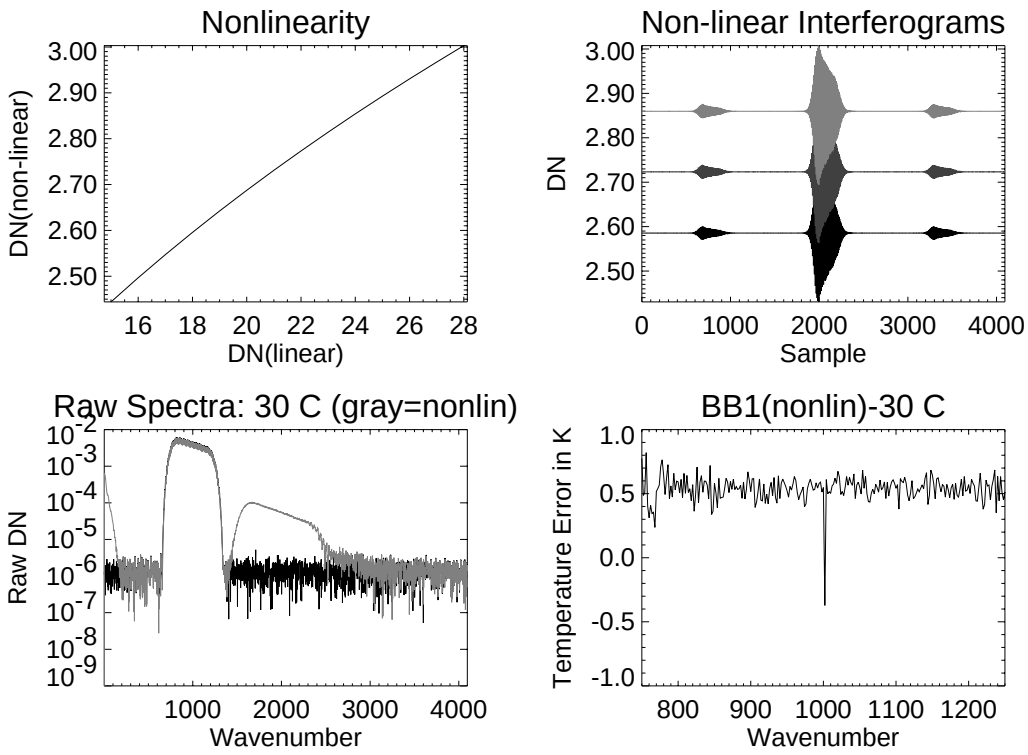

Figure 5. Non-linearity function DN(nonlinear) (UL), interferograms for 20^o, 30^o and 40^o C black-bodies (UR), the raw digital number (DN) spectrum for the 30^o C black-body with noise (LL), and the temperature error for the 2-point calibrated 30^o C black-body (LR).

Other methods are described in Richardson et al, 1998. Van Delst, has a nice write-up on correcting HgCdTe non-linearities for the AERI instrument at:
http://airs2.ssec.wisc.edu/∼paulv/aeri/aerinsa_nlanalysis/971113b1/971113b1.html.

4. GEOMETRIC CORRECTIONS

Imaging a scene from a moving platform or imaging a moving object with an imaging FTIR causes spatial information to be blurred. Point sources might become un-detectable. Thus it helps to register the interferogram cube frame by frame before the Fourier transform is performed.

Problem: Given a reference image $I(0)$ and a sequence of N x/y shifted and rotated images find the optimal shifts, $x_{opt}(n)$ and $y_{opt}(n)$ and rotation, $\phi_{opt}(n)$ to minimize:

$$RMSE(I(0) - \text{rotate}(\text{shift}(I(n), x_{opt}(n), y_{opt}(n)), \phi_{opt}(n))).$$

Possible Algorithms include direct 3-D cross correlations, direct 2-D cross correlations, adaptive (from low-resolution to high-resolution) 2-D image correlations, or separable 1-D correlations which can also handle small angle rotations. The advantages of last method over the previous ones are that only simple 1-D correlations need to be performed rather than computationally expensive 2 or 3-dimensional correlations and that small angular rotations can be handled which can otherwise be difficult to implement since traditional Fourier techniques produce a spurious peak near 0 deg (Lucchese et al, (1997)). These false peaks can be avoided using low-pass filtering on the images before performing the correlations (Stone et al (2001)). Codes for a hierarchical cross-correlation technique by Varosi can be found at: *http://idlastro.gsfc.nasa.gov/ftp/contrib/varosi/vlib/.*

4.1. Method for fast x/y shift determination based on projections

Independent from Alliney and Morandi, (1986) and probably others, we have developed a fast algorithm based on projections for determining x/y shifts with an accuracy to 1/20th of a pixel. A block-diagram for the method is shown in Fig. 11. Steps of the fast correlation algorithm:

1. Select a region with a feature and initialize a maximum search range R_0, e.g. +/- 5 pixels

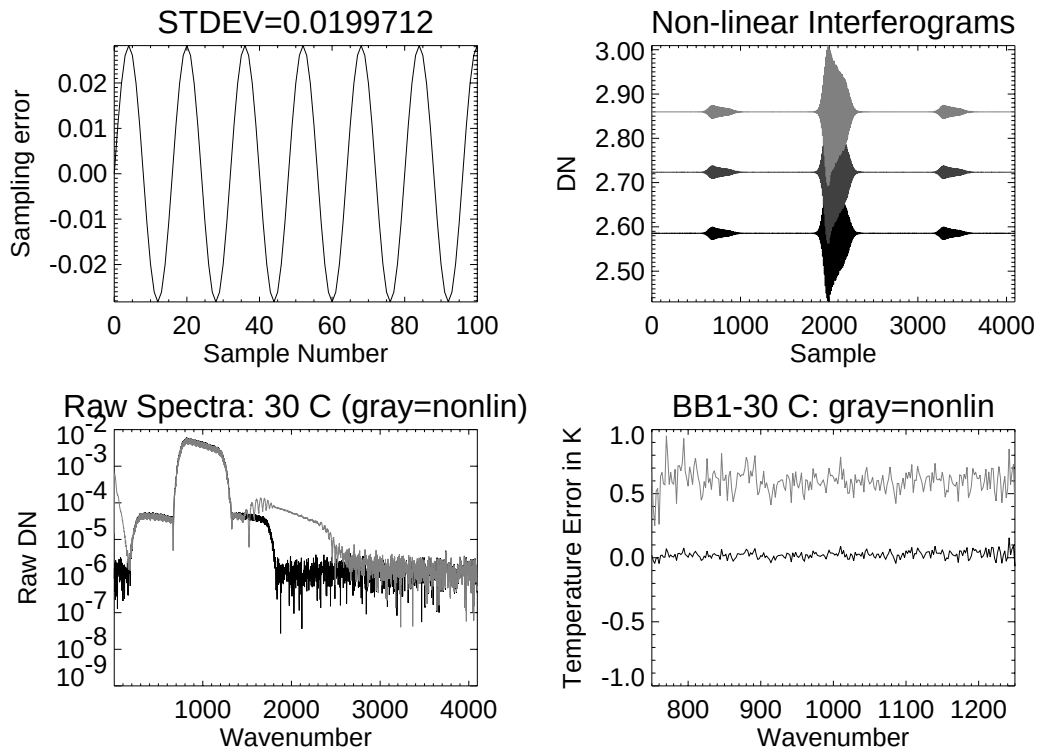

Figure 6. Periodic sample position error $\Delta Z_p(z)$ for 100 samples (UL), interferograms for 20^o, 30^o and 40^o C black-bodies (UR), the raw digital number (DN) spectrum for the 30^o C black-body with noise (LL), and the temperature error for the 2-point calibrated 30^o C black-body (LR).

2. Sum over all rows and columns of reference frame to obtain 1-D vectors $S_x(0) = \sum_x(I(0))$ and $S_y(0) \sum_y(I(0))$.
3. For frame n and k iterations do:
   (a) Let $x_{opt,0}(n) = x_{opt}(n-1)$ and $y_{opt,0}(n) = y_{opt}(n-1)$.
   (b) Cross-correlate 1-D vectors over a range of shifts from $-R$ to R in 11 steps: $S_x(n) = \sum_x \text{shift}(I(n), x_{opt}(n-1), y_{opt}(n-1))$, and $S_y(n) = \sum_y \text{shift}(I(n), x_{opt}(n-1), y_{opt}(n-1))$ with $S_x(0)$ and $S_y(0)$ to find residual shifts δ_x and δ_y which minimize $RMSE(S_x(0) - \text{shift}(S_x(n), \delta_x, \delta_y))$ and $RMSE(S_y(0) - \text{shift}(S_y(n), \delta_x, \delta_y))$.
   (c) Let $x_{opt,k}(n) = x_{opt,k-1}(n) - \delta_{x,k-1}$ and $y_{opt,k}(n) = y_{opt,k-1}(n) - \delta_{y,k-1}$.
   (d) Reduce the range by $R_k = R_{k-1}/2$.

4.2. Fast rotation determination

Steps:

1. Select a region of interest and initialize a maximum search angle range for Φ_0, e.g. +/- 5 degrees
2. Sum over all rows and columns of reference frame to obtain 1-D vectors $S_x(0) = \sum_x(I(0))$ and $S_y(0) \sum_y(I(0))$.
3. For frame n and k iterations do:
   (a) Let $\phi_{opt,0}(n) = \phi_{opt}(n-1)$.
   (b) Cross-correlate 1-D vectors over a range of angles from $-\Phi$ to Φ in 11 steps: $S_x(n) = \sum_x \text{rotate}(I(n), \phi_{opt}(n-1))$, and $S_y(n) = \sum_y \text{rotate}(I(n), \phi_{opt}(n-1))$ with $S_x(0)$ and $S_y(0)$ to find residual rotation angle $\delta\phi$ which minimize $RMSE(S_x(0) - \text{rotate}(S_x(n), \delta\phi)$.
   (c) Let $\phi_{opt,k}(n) = \phi_{opt,k-1}(n) - \delta\phi_{k-1}$.
   (d) Reduce the angular range by $\Phi_k = \Phi_{k-1}/2$.

The effect of the jitter on interferograms depends on the surrounding area as shown in a simulated scene in Fig. 12. Only if the jitter has high-frequency components will the spectrum of the pixel be altered.

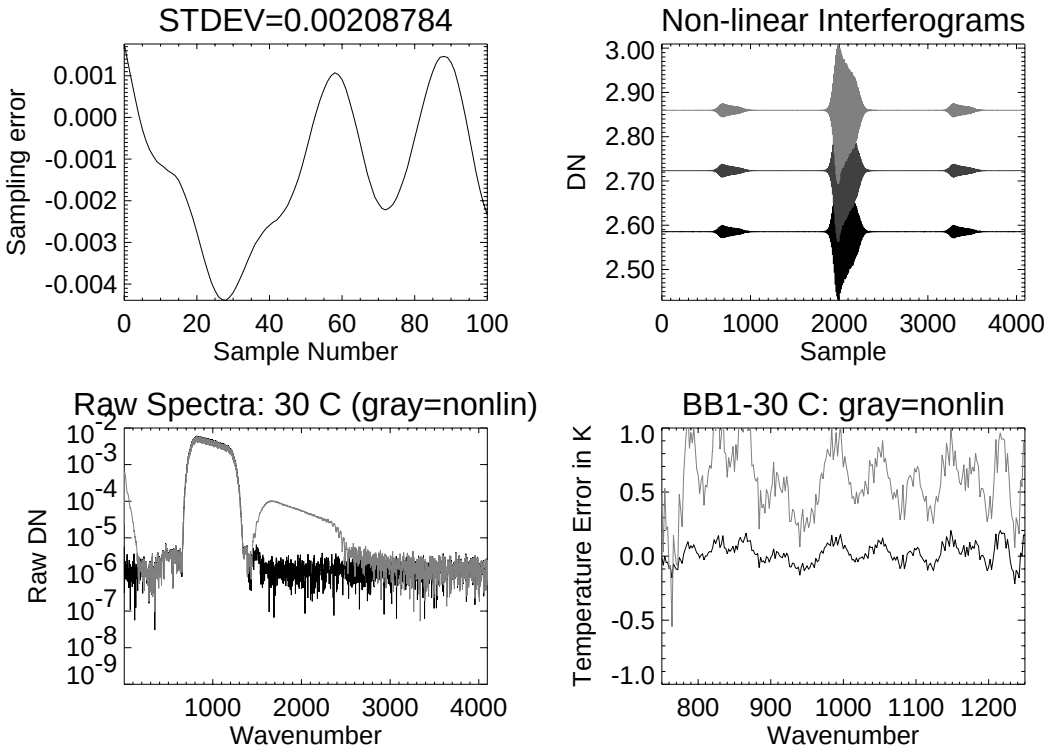

Figure 7. Random sample position error $\Delta Z_r(z)$ for 100 samples (UL), interferograms for 20^o, 30^o and 40^o C black-bodies (UR), the raw digital number (DN) spectrum for the 30^o C black-body with noise (LL), and the temperature error for the 2-point calibrated 30^o C black-body (LR).

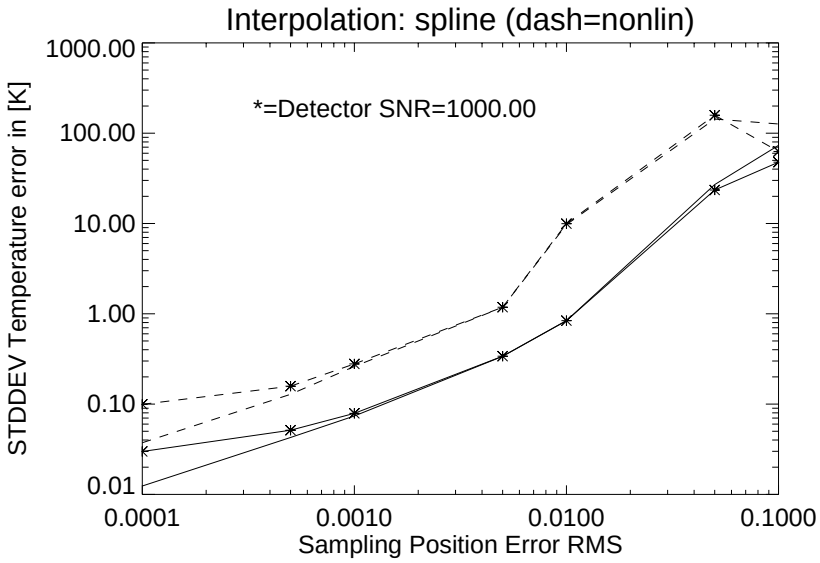

Figure 8. The effect of sample position errors, detector noise, and detector nonlinearities on temperature errors in FTIR's.

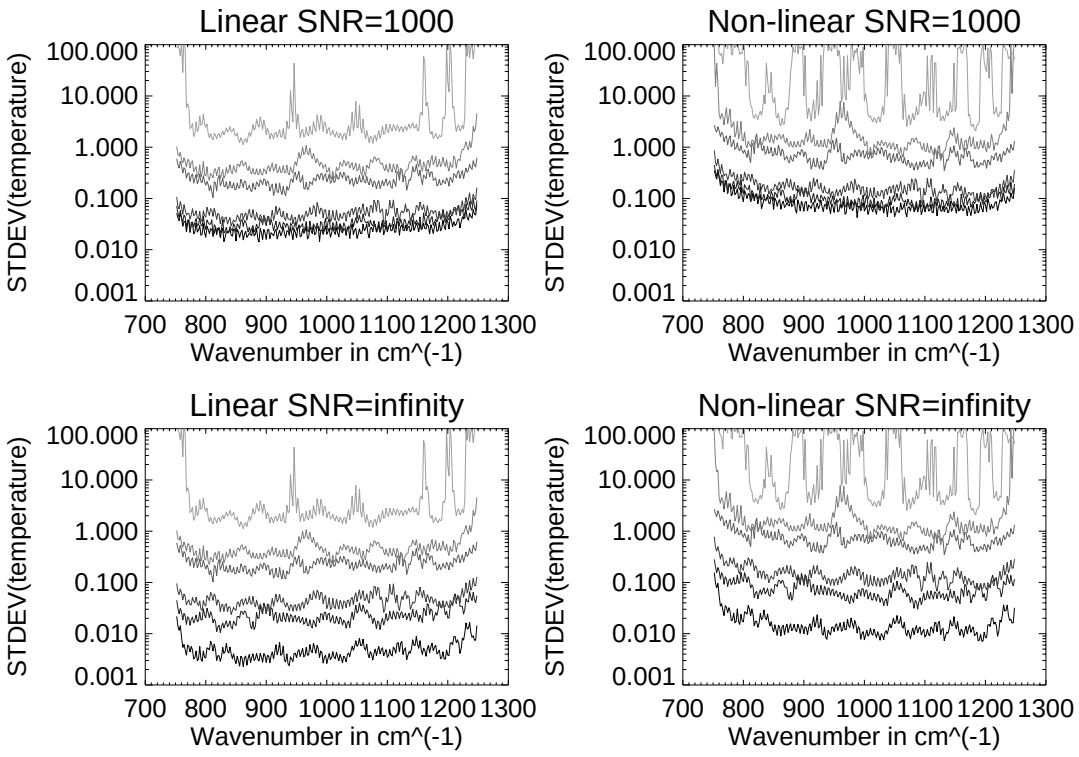

Figure 9. Spectral brightness temperature errors in BB_1 as a function of the standard deviation of the random sampling position error. The RMS sampling position error for the black to gray curves are: 0.0001, 0.0005, 0.001, 0.005, 0.01, 0.05 samples.

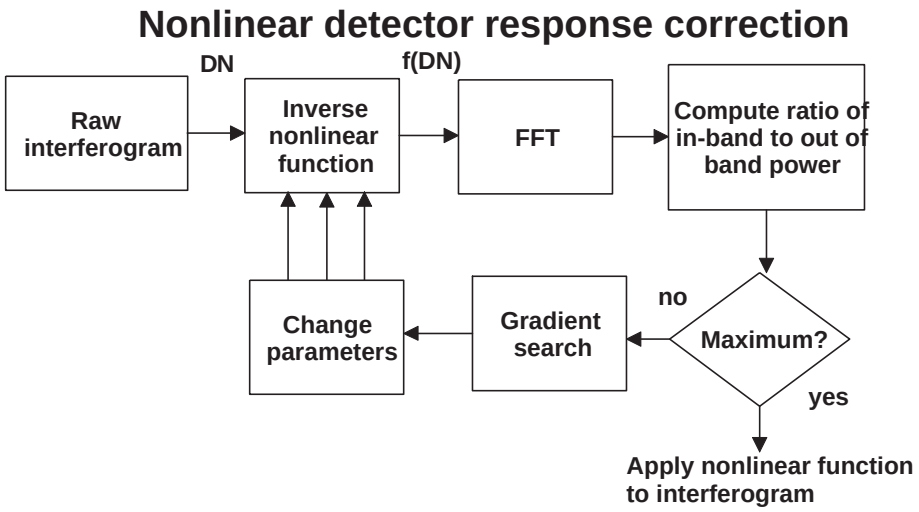

Figure 10. Removing non-linear distortions by maximizing the ratio of in-band to out-of-band signal.

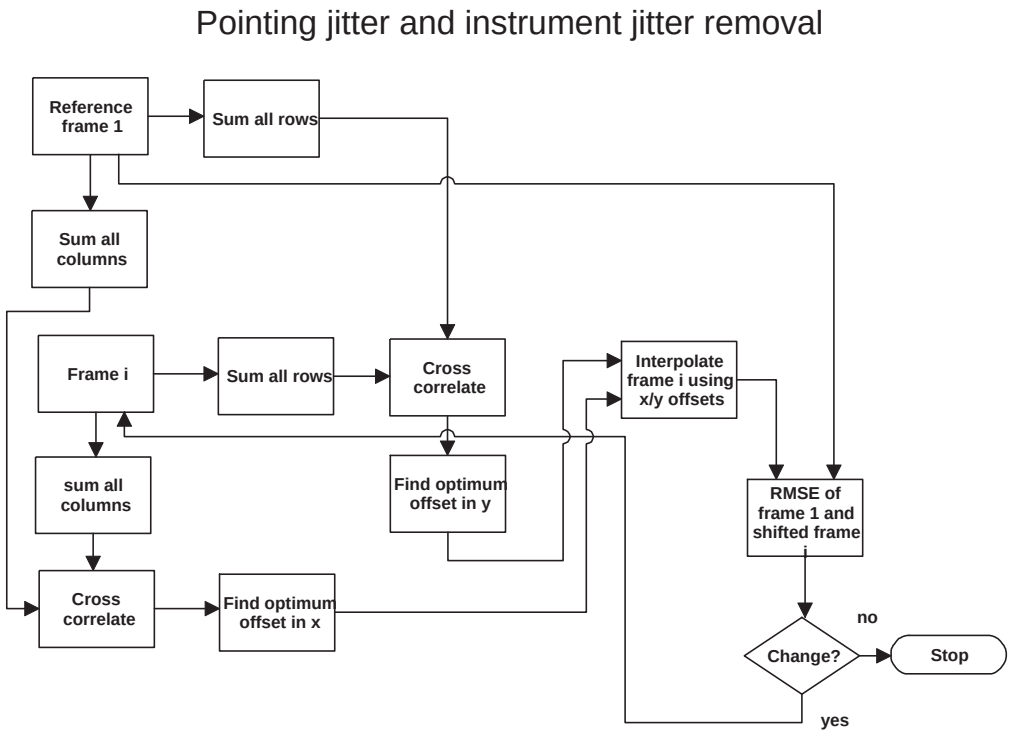

Figure 11. Block diagram for a fast tracking algorithm based on 1-d correlations of image projections.

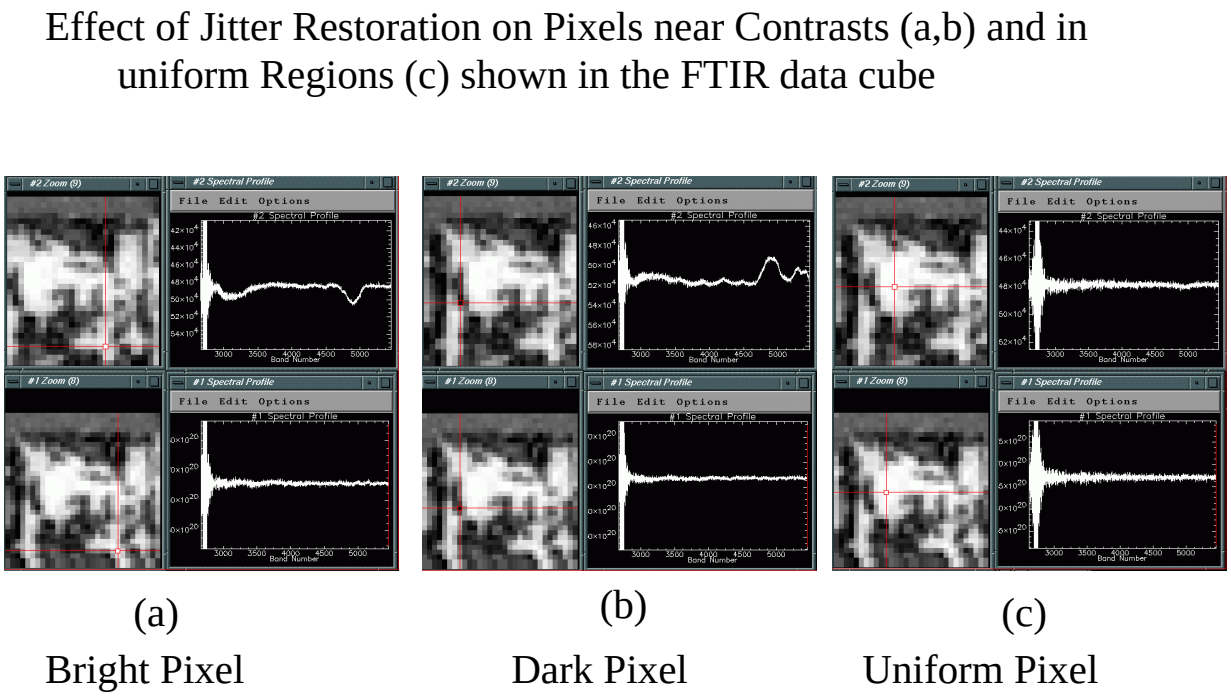

Figure 12. A bright pixel surrounded by dark pixels shows strong base line shifts (a), a dark pixel surrounded by bright pixels shows strong base line shifts (b), and a pixel in a uniform region shows no baseline shifts (c).

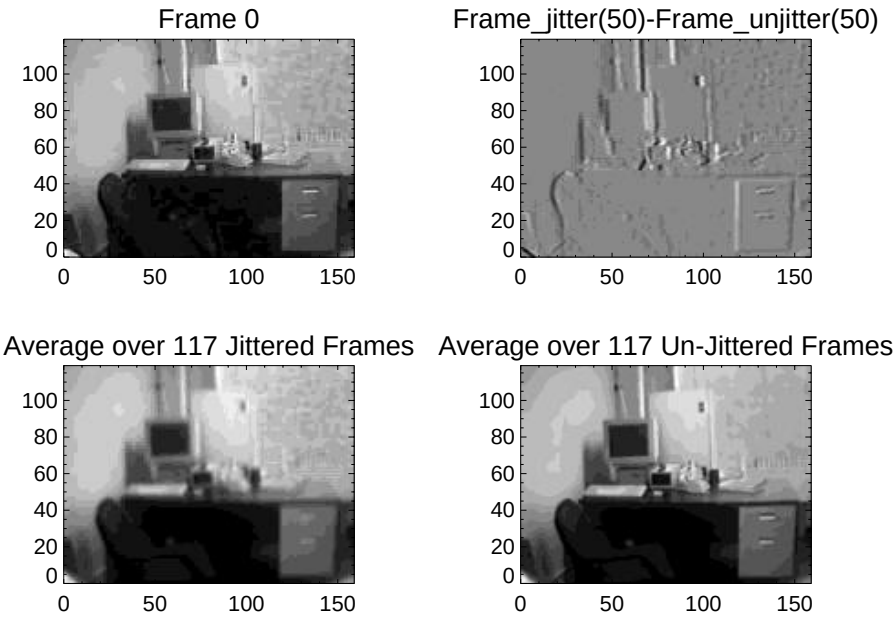

Figure 13. Effect of jitter and jitter corrected on overall image quality.

4.3. Results of three experiments

Experiment 1: This experiment is not performed on simulated FTIR data but on recorded 117 frames of video from camera placed on a shaking surface and tracked shifts and rotations. A small image region near the center of the image was selected for the estimation of translation and rotation. No post-processing was applied to the imagery. The average over the 117 jittered frames shows a blurred scene whereas the jitter corrected average resembles the reference frame 0. An animation of the original and corrected image sequence is available on: *nis-www.lanl.gov/∼borel*.

Experiment 2: Track motions for a simulated FTIR cube with random translations. We generated an ideal still simulated linear FTIR image cube C_0 and jittered each frame of the cube using a known jitter function $x_{off}(n)$ and $y_{off}(n)$ to obtain a cube C_j. Next we performed the jitter correction of the cube using the translational correlation technique described above and stored the result in image cube C_u. To compare the results in the spectral domain we Fourier transformed C_0, C_j and C_u and computed the averaged spectra for different regions over a region of 32 x 32 pixels as shown in Fig. 14. The jitter correction process has little effect on the spectral region of interest (500-800 arbitrary wavenumbers) but reduces the spurious signal near zero wavenumber.

Experiment 3: Tracking motions in a simulated FTIR cube. We use the simulated cube from Experiment 2 and determine the tracking error which is the difference between the estimated jitter function ($\hat{x}_{off}$, $\hat{y}_{off}$) and the simulated one. For this case the tracking error for shifts only, is less than one 10-th of a pixel. Note however that for imaging FTIR's with a sensor field of view greater than 1 degree we have to contend with fringes which are due to optical path differences between the center and the off-center pixels. They manifest themselves as bright and dark rings which make correlations almost impossible in the center-burst and channeling regions. We have recently found a method to remove these fringes for an un-compensated FTIR.

4.4. A method to fix bad pixels

Before image correlations can be performed bad pixels need to be identified and fixed. To fix bad pixels we grow a region around bad pixels using a cross shaped kernel. A Delauney triangulation of neighbor pixels is performed and we use a high-order (quadratic to quintic) interpolation over the bad pixels. This method is used in a program (fill_image.pro) written by Paul Ricchiazzi at UCSB available from: *ftp.icess.ucsb.edu:/pub/esrg/idl*.

5. CONCLUSIONS

Several "real world" effects on FTIR data have been presented and some methods to reduce these effects. Channeling removed by apodizing the interferogram introduces ringing near spectral lines. For a stable FTIR the channeling can be calibrated out. Random and periodic sample position error even if they are less than 1/100 of a sample can limit the temperature accuracy of a spectrometer to greater than 0.1 deg K. We also noted that

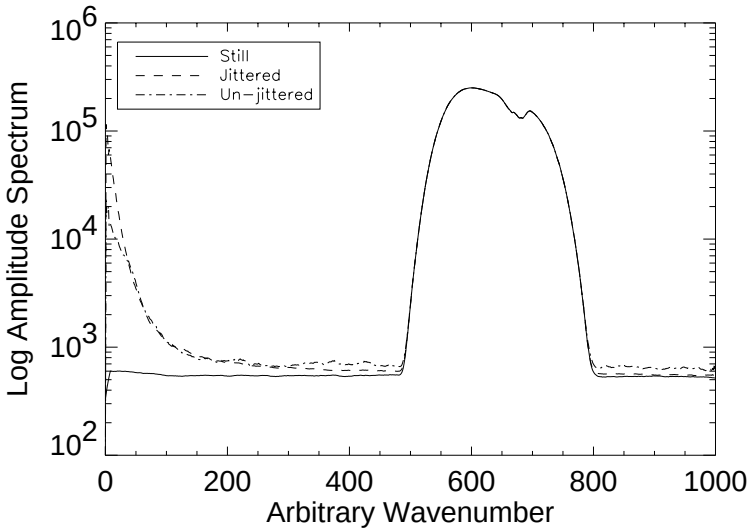

Figure 14. Average spectra of a still, jittered and jitter corrected image cube show that the spectrum is not altered but the low-frequency spectral features are smaller.

special care must be taken to reduce sampling position errors if the detector is non-linear. Non-linearity correction eliminates systematic calibration errors. Pointing jitter removal improves image sharpness but has little effect on spectral fidelity if the jitter is low-frequency.

References

Alliney, S. and C. Morandi, Digital image registration using projections, IEEE Trans. on Pattern Analysis and Machine Intelligence, Vol. 8, no. 2, pp. 222-233,1986.

Beer, R., *Remote sensing by Fourier transform spectrometry, Fourier transform spectroscopy, Remote Sensing,* 153 p., New York, N.Y., Wiley, 1992.

Bell, R.J., *Introductory Fourier transform spectroscopy*, Academic Press, 1972.

Peter R. Griffiths and James A. de Haseth, *Fourier transform infrared spectrometry,* xv, 656 p., New York, Wiley, 1986.

Bennett, C.L., LIFTRS, the Livermore imaging FTIR, Conference on Fourier transform spectroscopy, 11., p.170-186, 10-15 Aug, 1997.

Hackwell, J.A. et al, LWIR/MWIR imaging hyperspectral sensor for airborne and ground-based remote sensing, Proc. SPIE, Vol. 2819, 1996.

Learner, R.C.M., A.P. Thorne and J.W. Brault, Ghosts and artifacts in Fourier-transform spectrometry, Appled Optics, Vool. 35, no. 16, 1996.

Lucchese, L., Cortelazzo, G.M., Monti, C., High resolution estimation of planar rotations based on Fourier transform and radial projection, ISCAS '97., Proceedings of 1997 IEEE International Symposium on Circuits and Systems, 1997.

Manning, C.J. and P.R. Griffiths, Noise sources in step-scan FTIR, Applied Spectroscopy, , Vol. 51, no. 8, pp. 1092-1101, 1997.

MacBride, D.M., C.G. Malone, J.P. Hebb and E.G. Cravalho, Effect of temperature variation on FT-IR spectrometer, Applied Spectroscopy, , Vol. 51, no. 1, pp. 43-50, 1997.

Richardson, R.L., H. Yang and P. Griffiths, Evaluation of a correction for photometric errors in FT-IR spectrometry introduced by a nonlinear detector response, Applied Spectroscopy, Vol. 52, no. 4, 1998.

Stone, H.S., B. Tao, M. McGuire, Analysis of image registration noise due to rotationally dependent aliasing, submitted for publication, 2001.

Palchetti, L. and D. Lastrucci, Spectral noise due to sampling errors in Fourier-transform spectroscopy, Vol. 40, no. 19, pp. 3235-3243, 2001.